

Entanglement topological invariants for one-dimensional topological superconductors

P. Fromholz^{1,2,*}, G. Magnifico^{1,3,4,*}, V. Vitale^{1,2}, T. Mendes-Santos^{1,2} and M. Dalmonte^{1,2}

¹The Abdus Salam International Centre for Theoretical Physics, Strada Costiera 11, 34151 Trieste, Italy

²SISSA, via Bonomea 265, 34136 Trieste, Italy

³Dipartimento di Fisica e Astronomia dell'Università di Bologna, I-40127 Bologna, Italy

⁴INFN, Sezione di Bologna, I-40127 Bologna, Italy



(Received 7 October 2019; revised manuscript received 6 February 2020; accepted 7 February 2020; published 24 February 2020)

Entanglement provides characterizing features of true topological order in two-dimensional systems. We show how entanglement of disconnected partitions defines topological invariants for one-dimensional topological superconductors. These order parameters quantitatively capture the entanglement that is possible to distill from the ground-state manifold and are thus quantized to 0 or $\log 2$. Their robust quantization property is inferred from the underlying lattice gauge theory description of topological superconductors and is corroborated via exact solutions and numerical simulations. Transitions between topologically trivial and nontrivial phases are accompanied by scaling behavior, a hallmark of genuine order parameters, captured by entanglement critical exponents. These order parameters are experimentally measurable utilizing state-of-the-art techniques.

DOI: [10.1103/PhysRevB.101.085136](https://doi.org/10.1103/PhysRevB.101.085136)

I. INTRODUCTION

Recently, entanglement has emerged as a groundbreaking diagnostic to characterize and classify many-body quantum phenomena in and out of equilibrium [1–4]. An archetypal example is the possibility of unambiguously detecting topological order in two-dimensional systems via the topological entanglement entropy (TEE) [5–7]. The latter spots the presence of “long-range” entanglement which is not distillable via local operations; consequently, it defines a genuine entanglement order parameter that distinguishes phases depending on their quasiparticle content [8]. This insight has been widely employed in the characterization of topologically ordered states in numerical simulations [9–11] and has stimulated the search for experimentally realistic entanglement probes [12–18].

While the definition of the TEE naturally emerges from gauge theories in two dimensions, the existence of topological invariants based solely on entanglement properties in one-dimensional (1D) topological matter, e.g., in the form of an order parameter, is presently not clear. In 1D, bipartite entanglement of *connected* partitions does not display informative scaling corrections [2,3]. Its finer structure—captured by the entanglement spectrum—provides sharp *sine qua non* [19–21], but even the entanglement spectrum of single partitions is not able to distinguish the topological character of wave functions [22]. Indeed, at the field-theory level and in 1D, connected bipartite entanglement is strongly influenced by ultraviolet contributions due to edges and is thus not immediately linked to “universal” information.

In this paper, we show how entanglement and Rényi entropies of *disconnected partitions* provide a set of entanglement order parameters for 1D topological superconductors (TSCs) [24,25]. These order parameters satisfy the following properties: (i) they are quantized to 0 or $\log 2$ when the phase is topologically trivial or nontrivial, respectively, and are thus able to detect the single entanglement bit—an ebit—that can be distilled from the ground state manifold; (ii) they display a scaling behavior when approaching quantum phase transitions, thus defining entanglement critical exponents that describe the build-up of nonlocal quantum correlations across such transitions; (iii) some of them are experimentally measurable in and out of equilibrium, utilizing recently introduced [14,15] and demonstrated [26] techniques based on random measurement methods [27].

Following Ref. [28], we consider the F function between two partitions A, B , which compensate for all edges and volume contributions in an open chain of length L . These properties are required to avoid nonuniversal effects: The significance of our diagnostics relies on an underlying gauge theory description below, which calls for quantities that are divergence-free in the continuum limit. To diagnose the presence of nonlocal correlations in the system, we choose two partitions with *different connectivity*, as shown in Fig. 1(a). The resulting disconnected n -entropies S_n^D read

$$S_n^D = S_{A,n} + S_{B,n} - S_{A \cup B,n} - S_{A \cap B,n}, \quad (1)$$

where $S_{F,n}$ is the bipartite Rényi entropy of order n of the partition $F = A, B, A \cup B$ or $A \cap B$. We define L_α as the size of a given partition and L_D as the distance between the two different parts of B . Unless stated otherwise, we consider the representative case $L_A = L_B$, which provides a cleaner finite-size scaling analysis.

We denote the case $n = 1$ as S^D , that corresponds to the von Neumann entropy, and satisfies $S^D > 0$ because of

*These authors contributed equally to this work.

†Corresponding author: fromholz@ictp.it

‡Corresponding author: g.magnifico91@gmail.com

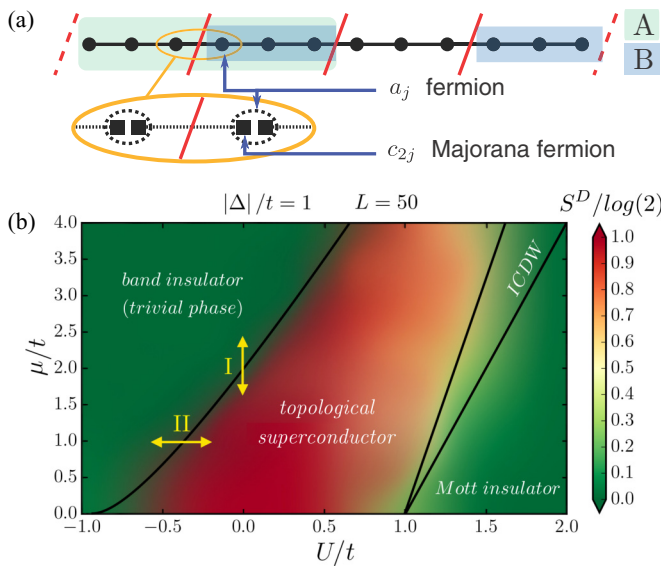


FIG. 1. Partitions associated with the entanglement topological order parameter and the phase diagram of the interacting Kitaev chain. (a) schematics of the partitions A (shaded, green) and B (shaded, blue) considered here. Each site of the chain hosts a spinless fermion degree of freedom, a_j , that can be decomposed into two Majorana fermions c_{2j} and c_{2j+1} . The orange circle magnifies the cut across partitions: Deep in the topological phase, neighboring Majorana fermions belonging to different physical sites are coupled (dashed line). The partition cut takes place exactly between the two coupled Majorana fermions. (b) disconnected von Neumann entropy S^D as a function of μ/t , U/t , at fixed $\Delta = 1$. Black lines are from Ref. [23]. The color plot is obtained via interpolation on a 5×7 grid. Clearer evidence of the quantization of S^D in a phase and the sharpness of the transition requires a lot of points, as we highlight on lines I and II in Sec. III B.

strong subadditivity. This entropy improves from Ref. [29] that uses two systems with different boundary conditions. It has been considered in Ref. [30], which pointed out a strong analogy between bosonic symmetry-protected topological phases (SPTs) and error-correcting codes. Here, we focus instead on fermionic phases where topology stems from an underlying fundamental symmetry (parity) which cannot be broken by any Hamiltonian perturbation. This condition plays a crucial role in defining the upcoming gauge-theory picture describing the entanglement content of such states while the nonlocal correlations introduced by the fermionic algebra via the Jordan-Wigner string are responsible for such analogy.

At a qualitative level, the key in S_n^D is the disconnected partition B : All other terms are complementary, and only required to eliminate nonuniversal boundary and volume terms. In Fig. 1(b), we show the finite-size behavior of S^D across the phase diagram of interacting Kitaev chains: This plot illustrates graphically how, even at modest system and partition sizes, S^D clearly distinguishes topological from trivial phases. We note that Ref. [31] computes a quantity coinciding with S_n^D for the noninteracting Kitaev chain, but it should deviate when a quantum spontaneous symmetry breaking phase is involved.

The present study is divided into the theoretical part Sec. II and the computational part Sec. III. The first part introduces shortly the Kitaev model (Sec. II A). Then, it both derives and gives an intuitive picture of entanglement and the topological order parameter S^D in the deep topological or trivial regime (Sec. II B) and using lattice gauge theories (Sec. II C). The computational part displays the efficiency of S^D as a topological detector (Sec. III A), reveals its universal behavior at the transition (Sec. III B), shows its response to quenches which is typical of a topological invariant (Sec. III C), and confirms its robustness to symmetry-preserving disorder (Sec. III D). We then discuss the existing experimental relevancy of the detector in Sec. IV A before concluding. The Appendices mirror the main structure of the paper and add miscellaneous details referred to in the text. In particular, Appendix A 1 provides a longer introduction on the Kitaev wire for the unfamiliar reader while Appendix A 3 attempts a proof of the equivalence between all S_n^D as topological detecting quantities.

II. DISCONNECTED ENTROPY OF THE INTERACTING KITAEV WIRE

The Kitaev wire gives a prime example of a topological phase in 1D, with well-known behavior deep into either the topological or trivial phase. There, a topological signature is more easily extracted and identified from the entanglement of a ground state. An analytical treatment is possible and presented here.

A. The model Hamiltonian

We consider the interacting version of a Kitaev p -wave superconductor, whose Hamiltonian reads

$$H = \sum_{j=1}^{L-1} \left[-t(a_j^\dagger a_{j+1} + \text{H.c.}) + (\Delta a_j a_{j+1} + \text{H.c.}) \right. \\ \left. + 4U \left(n_j - \frac{1}{2} \right) \left(n_{j+1} - \frac{1}{2} \right) \right] - \mu \sum_{j=1}^L n_j, \quad (2)$$

where a_j^\dagger (a_j) are the creation (annihilation) operators of the spinless fermion on site j , $n_j = a_j^\dagger a_j$, t is the hopping amplitude, Δ is the superconducting amplitude, U is the nearest-neighbor interaction, and μ is the chemical potential. The phase diagram of the model is known [23,32] and displays a TSC phase, in addition to topologically trivial phases, including a band insulator, a Mott insulator, and an incommensurate charge-density-wave (ICDW) phase. For any state in the Hilbert space, the bipartite properties of a simply connected partition are equivalent to the ones of the XYZ spin chain obtained from Eq. (2) after applying a Jordan-Wigner transformation. As such, they are uninformative about the topological origin of a given phase.

B. Disconnected entropies at exactly soluble points

Therefore, the goal is to find a combination of entropies able to both unambiguously capture the influence of nonlocality in the ground-state properties and identify the amount of information—in this case, a single ebit—that can be stored

in the ground-state manifold. The goal is reached for S^D , which contains the simplest nontrivial disconnected partition, S_B while all other terms only compensate possible volume and edge effects.

For conformal phases, S_n^D is immediately given by conformal field theory [2,33,34] and vanishes in the thermodynamic limit. For gapped phases, one has to distinguish between topologically trivial and nontrivial phases. We analyze here the limiting cases.

(i) $t = \Delta = U = 0, \mu > 0$: The system is a band insulator, and the density matrix of arbitrary partitions has rank 1 both in fermionic and spin systems. This immediately gives $S_n^D = 0$. The same result holds in the Mott insulator phase. Thus, the thermodynamic limit of S_n^D cannot distinguish conformal phases and trivial phases. Only the finite size correction of S_n^D may distinguish them.

(ii) $t = \Delta = 1 \gg |\mu|, U = 0$: This regime is representative of the TSC phase. Its correspondent in the XYZ model is a ferromagnetic phase, which we analyze first as a representative of a symmetry-broken phase. There, the lowest energy states at any finite size are equal weight superpositions of the two ferromagnetic states, $|\Psi_{XYZ}\rangle = (|\uparrow\uparrow\uparrow\dots\rangle \pm |\downarrow\downarrow\downarrow\dots\rangle)/\sqrt{2}$, separated by a gap $\delta \propto e^{-L}$. For both states, any reduced density matrix of an arbitrary spatial partition is equivalent, and thus $S_n^D = 0$.

For the TSC, the situation is different. While $S_A, S_{A \cap B}, S_{A \cup B}$ are the same as in the spin model, S_B has a sharply different behavior. In this regime, the ground state is twofold degenerate (again, up to a gap $\delta \propto e^{-L}$): Each of the two states $|\Psi\rangle_{\pm}$ can be written as an equal weight superposition of states with a given parity $|\psi\rangle_{\pm}$, i.e., $|\Psi\rangle_{\pm} = (1/2^{L-1}) \sum_{\psi} |\psi\rangle_{\pm}$. The proper fermionic trace evaluates the entanglement structure of arbitrary partitions so we obtain $S_B = 2 \log 2$. This returns a disconnected entropy $S^D = \log 2$. A full derivation is given in Appendix A 2.

The behavior of these cartoon wave functions sharply distinguishes the TSC phase with respect to all other phases. We need to go beyond these cartoons to understand if this behavior is a property of a phase, and if the value of S^D remains quantized in the whole TSC phase. Before presenting numerical results in support of these findings, we now illustrate how the quantization of S^D emerges naturally when utilizing a lattice gauge theory (LGT) description of the Kitaev chain.

C. Gauge theory characterization of entanglement properties.

The starting point is the exact relation [35] between Eq. (2) and a \mathbb{Z}_2 LGT, that we schematically review. The \mathbb{Z}_2 LGT describes the coupling between the \mathbb{Z}_2 gauge fields residing on bonds (represented here by Pauli matrices, $\sigma_{j,j+1}^z$), and the hard-core Higgs fields φ_j , with $n_j = \varphi_j^\dagger \varphi_j$, defined on the vertices. The gauge-invariant Hilbert space is defined as the set of states where the local parity $P_j = (1 - 2n_j)\sigma_{j-1,j}^z \sigma_{j,j+1}^z$ is fixed to 1 (see Fig. 2). Under open boundary conditions (OBCs), we fix to $\sigma_{0,1}^z = 1$ the value of the first gauge field without loss of generality. The value of the last gauge field $\sigma_{L,L+1}^z = P$ gives the total parity of the system due to gauge invariance.

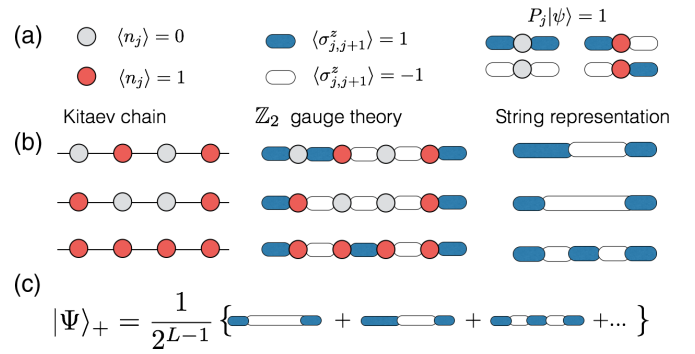


FIG. 2. Schematics of the correspondence between the Kitaev chain and \mathbb{Z}_2 lattice gauge theories. (a) Hilbert space structure and gauge-invariant building blocks. (b) Three examples of the mapping between states in the fermionic (left), gauge theory (center), and string representation (right). (c) String representation of $|\Psi\rangle_+$.

The ground-state wave functions $|\Psi\rangle_{\pm}$ can be described in terms of either fermionic or gauge fields, since, in 1D, those are mutually fixed by Gauss law. In terms of LGT, the ground states are equal-weight superpositions of all possible string states of arbitrary length and compatible with the boundary conditions: A sample of those are depicted in Fig. 2 for the case $P = 1$. This picture describes a 1D gauge theory in a phase with strongly fluctuating gauge fields, and is strongly reminiscent of the loop description of 2D quenched \mathbb{Z}_2 LGT [8,36,37].

Evaluating entanglement entropies in this phase is straightforward by exploiting gauge invariance:

(i) The entropy of each connected partition is $\log 2$. Indeed, let us define σ_L^z, σ_R^z as the two boundary spins of the partition. Their product is equal to the parity of the partition: The density matrix of the partition is block-diagonal in this conserved quantum number. If the correlation length is much smaller than the partition length, both positive and negative parities are equally probable and all states count with equal weight. The corresponding von Neumann entropy is thus $\log 2$.

(ii) The entropy of disconnected partitions is $(N_c - 1) \log 2$, where N_c is the number of partitions such that $N_c = 2$ corresponds to the standard bipartition of the chain into two halves. Indeed, let us define as $\sigma_{L,h}^z, \sigma_{R,h}^z$ the gauge fields at the boundaries of the partition h . As long as the length of each partition is larger than the correlation length, each patch is an equal-weight superposition of all possible states, under the condition that $P_h = +1$ or -1 for partitions with or without an outgoing flux, respectively. For a fixed total parity, there are 2^{N_c-1} finite, equal values of the corresponding density matrix, which returns an entropy equal to $(N_c - 1) \log 2$.

We emphasize that the gauge theory description enables a simple calculation of the entropies (by replacing fermionic statistics with a \mathbb{Z}_2 gauge field) and, at the same time, provides a simple, compelling physical picture, that might be extended to more exotic types of order.

III. S^D AS A TOPOLOGICAL INVARIANT ORDER PARAMETER

S^D is efficient as a topological order parameter even for modest system sizes. Indeed, we simulate the quantity and

obtain a sharp phase diagram of the Kitaev wire. Sharp, because close to the phase transition, it displays universal behavior typical of an order parameter and allows definition of critical entanglement exponents. Its characteristics as a topological invariant are confirmed by its invariance after a quench as expected from Sec. II C and by its robustness to disorder.

A. Scaling of S^D and phase diagram

We therefore turn to the numerical investigation of Eq. (2). We used free fermion techniques [38] to investigate the non-interacting case $U = 0$ and density-matrix-renormalization group (DMRG) [39,40] for $U \neq 0$. Since DMRG does not give immediate access to S_B , we performed separate simulations to obtain this quantity by modifying the lattice connectivity (cf. Appendix B 3). We kept at least 1200 states after truncation and performed at least 30 sweeps. Typical discarded weights at the end of the simulation were of order 10^{-8} .

The phase diagrams in Figs. 1(b) and 3(a) (with and without interactions) show how, even at very modest partition sizes, S^D is large and finite only the TSC phase. Comparison between Figs. 3(a) and 3(b) shows the equivalence between S^D and S_2^D . In Fig. 4(a), we show the finite-size-scaling behavior of S^D for representative points in the TSC ($\mu/t = 1.0, 1.5$) and topologically trivial ($\mu/t = 4$) phase. The asymptotic values are quantized within numerical accuracy of our fits to $\log 2$ and 0, respectively, in agreement with the theoretical discussion above. Fig. 4(b) shows how, in the TSC phase, quantization is approached exponentially fast in system size; the same holds true for S_n^D .

B. Universal behavior and entanglement critical exponents.

Since S^D captures universal properties of each phase, it is natural to wonder whether such quantities can display universal scaling behavior when crossing a quantum phase transition. Here, we focus on the transition between TSC and band insulator, which belongs to the Ising universality class.

Similar to conventional quantum critical behavior, we fit S^D using a phenomenological finite-size scaling ansatz,

$$S^D L^{\frac{a}{b}} = \lambda(L^{\frac{1}{b}}(\alpha - \alpha_c)), \quad (3)$$

where $\alpha = \mu$ or U is the varying parameter chosen, a and b (*a priori* different depending on the chosen parameter) take place of the usual critical exponent β and ν , and $\lambda(x)$ is a scaling function. We extract these parameters using curve intersections and collapse shown in Figs. 5 across the transition indicated in Fig. 1 with the yellow arrows (I) and (II). The results of the collapse scaling locates correctly the transition point (with errors 10^{-4}). Most surprisingly, we find that the entanglement critical exponents satisfy $a = b = 1$ irrespectively of where the transition line is crossed, a sharp signature of universal behavior. The quality of the collapse scaling in the interacting case is already good for modest system sizes, further corroborating such universal behavior.

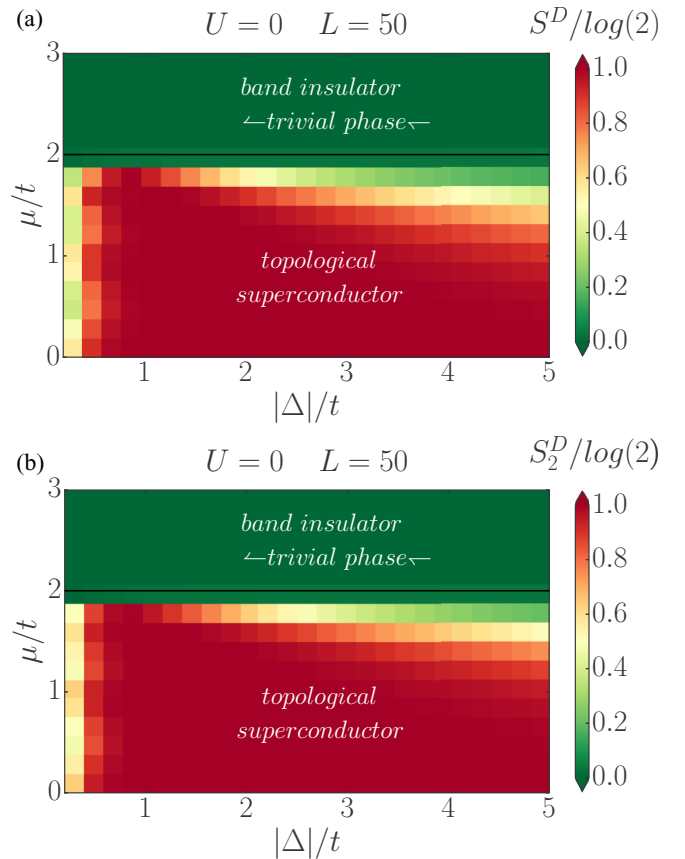


FIG. 3. Color plot of the disconnected n entropies, S_n^D , of the Kitaev wire without interaction, $U = 0$, for (a) $n = 1$ and (b) $n = 2$. The results are obtained with the free-fermion technique. The y axis represents the chemical potential, μ/t , while the x axis the superconducting amplitude, $|\Delta|/t$. A grid with 16×30 points is considered. The two theoretically expected phase transition lines occur for $|\Delta| = 0$ and $\mu/t = 2$, respectively. Using the definitions of Fig. 1(a), $L = 50$, $L_A = L_B = 12$, and $L_D = 32$. The diagrams coincide with the results obtained in Ref. [31].

C. Invariance of S^D under coherent dynamics.

In the thermodynamic limit, topological invariants cannot change under unitary evolution (as long as specific symme-

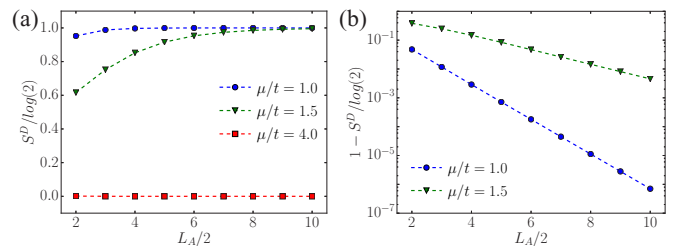


FIG. 4. Finite-size scaling properties of S^D in (a) normal scale, (b) log scale, for a chain with $L_A = L_B = (L_{A \cap B} + L_{A \cup B})/2$, and $U = 0$, $\Delta/t = 1$. In the topologically trivial phase, S^D quickly vanishes. In contrast, in the topological phase ($\mu = 1.0, 1.5$), S^D increases as a function of system size, and approaches its thermodynamic value exponentially fast when increasing L_A , as shown in (b).

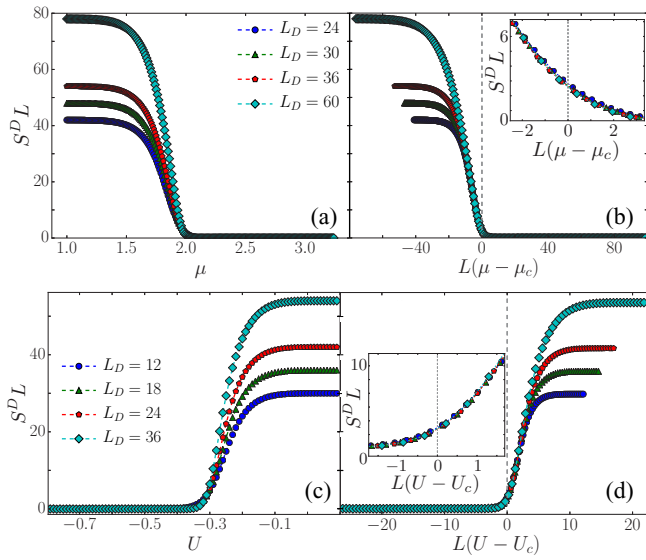


FIG. 5. Finite size scaling of S^D (in units of \log_2) along lines (I) and (II) of Fig. 1 as a function of L_D and μ or U using DMRG. In all plots, $L_A = L_B = 12$. (a) $S^D L$ as a function of μ for different sizes: The critical value μ_c is the intersection of all curves; we obtain $\mu_c = 1.978$. (b) Scaling of $\lambda(x)$ for different system sizes: Curve collapse. The collapse is best realized for $a = b = 1$, values that also minimize the square root of the residual sum of squares. (c) $S^D L$ as a function of U for different sizes: The critical value is here $U_c(12) = -0.314$. (d) The collapse is again best realized for $a = b = 1$. Simulations with more sites (especially using free fermion techniques) only confirm these results.

tries are not broken explicitly [41–43]). To check that S^D is a true topological invariant, we performed an extensive investigation based on quantum quenches within and across the topological phase.

A representative sample of our results is presented in Fig. 6. In panel (a), we plot the time evolution of S^D for a quench from an initial value of the superconducting amplitude $\Delta = 0.5$ to a final value $\Delta = 1.5$. Different lines correspond to different system sizes. For each size, one can sharply distinguish two regimes. At short times, S^D does not change with time and exhibits a plateau up to a time t_c that depends on L_A . After this timescale, quantization is lost, and the dynamics is dictated by nonuniversal dynamics. To understand whether quantization is a robust feature, we perform a finite-size scaling analysis in Fig. 6(d): Our results show that t_c (defined as the time when $S^D = 0.95$) grows approximately linearly with system size and will diverge at the thermodynamic limit. This behavior confirms the topological invariant nature of S^D . Figures 6(b), 6(c), 6(e), and 6(f) confirm these results for the quench $\mu_0 = 1.0$ to $\mu = 3.0$ (from topological to trivial) and $\mu_0 = 3.0$ to $\mu = 1.0$ (from trivial to topological). For Fig. 6(f), t_c is the time when $S^D = 0.05$.

D. Robustness of S^D to disorder

In 1D, the effect of disorder is the most drastic: Localization of the wave function occurs as soon as disorder exists, and not even diffusive transport is possible [44]. Topological

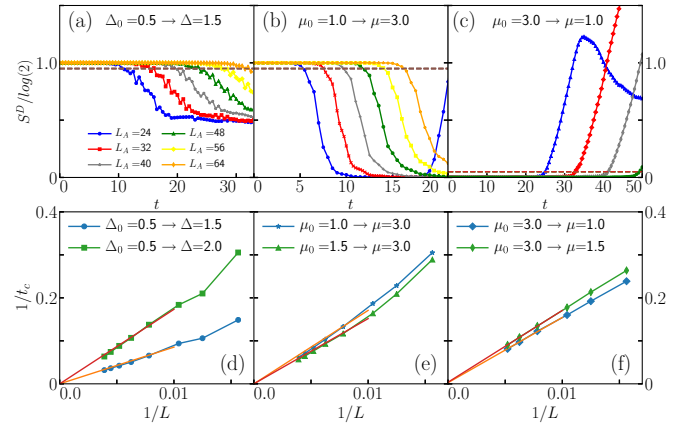


FIG. 6. Time evolution of S^D after a quantum quench from (a) $\Delta_0 = 0.5$ to $\Delta = 1.5$, (b) from $\mu_0 = 1.0$ to $\mu = 3.0$, and (c) from $\mu_0 = 3.0$ to $\mu = 1.0$ with $U = 0$, $\mu = 0$, $L = 8L_A$. Finite-size scaling of t_c or t'_c for two values of (d) Δ , (e) μ_0 , and (f) μ of the quenched Hamiltonian. In all cases, the width of the plateau diverges linearly with system size, as expected for topological invariants. The threshold lines of S^D according to the definition of t_c are depicted as a dashed line.

insulators and superconductors escape the effect, in the sense that their extended edge states stay robust against symmetry-preserving disorder. The same disorder should also preserve S^D that relies on these edge states. Numerical simulations indeed confirm the robustness of S^D to disorder for the noninteracting Kitaev wire.

We introduce finite Anderson-like disorder using

$$\mu_i = \mu + \delta_i, \quad \delta_i \in [-W/2; W/2], \quad (4)$$

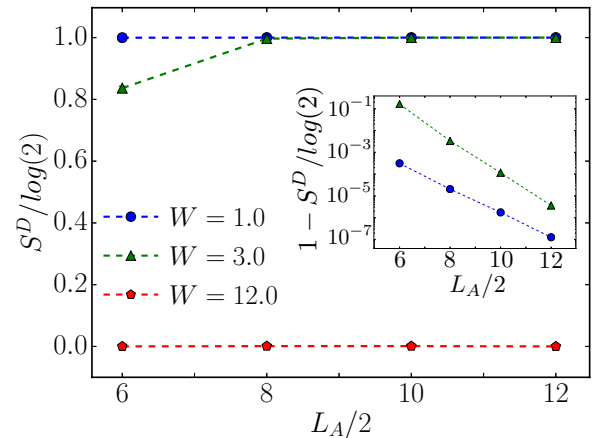


FIG. 7. Scaling in system size of the mean value of SD for $t = \Delta = \mu = 1$, $U = 0$, $L_A = L_B = (L_{A \cap B} + L_{A \cup B})/2$ and for three amplitudes of disorder: $W = 1$ and 3 in the topological phase and $W = 12$ for the trivial disordered phase (200 realizations of the disorder for each point). The inset provides a logarithmic scale for the axis of S^D : The scaling is exponential. The standard deviation is smaller than 10^{-6} for each point. The same study using Rényi-2 entanglement entropies leads to the same results quantitatively. The phase transition is expected at $W_c \sim 11$ for these parameters [45,46].

where μ_i is now the position-dependent (i) chemical potential in the Hamiltonian Eq. (2) (with $U = 0$). δ_i is a random variable of uniform distribution and W is the amplitude of the disorder. This potential breaks the translation symmetry, but not the protecting symmetries of the topological phase that persists for a reasonable amplitude of the disorder. In Fig. 7, we draw the mean value of S^D over realizations of disorder for different W as we increase the system size L . S^D scales exponentially in system size toward the quantized value of $\log 2$ for the topological phase, 0 otherwise.

IV. DISCUSSION AND CONCLUSIONS

A. Experimental measurement and comparison to other diagnostics.

The probes S_n^D are experimentally relevant because they are already informative for modest partition sizes, and because Rényi entropies can be measured. The proposals in Ref. [14] discuss how to perform measurements of Rényi-2 entropies in synthetic quantum systems: The complexity of the measurements is not sensitive to the connectivity of the partition itself, but only to its total size. Given that a large L_D allows the distillation of the correct information from the wave function, measuring S^D is as complex as measuring its largest partition A . We note that partitions of sizes up to ten spins have already been probed in experiments [26].

Finally, we comment on the relation between S^D and other diagnostics. Topological invariants such as the many-body Chern number [4,47] are unrelated to bipartite entanglement properties, as they do not depend solely on the spectrum of density matrices but also on their eigenfunctions. For specific symmetries, specific topological invariants can be defined [37,48–52] (and potentially experimentally measured [53]) also utilizing the matrix-product-state (MPS) classification of SPTs; these quantities are genuinely sensitive to the response of a state to specific (symmetric) operations and not immediately connected to entanglement. From a theoretical viewpoint, all these diagnostics represent complementary tools that give access to qualitatively different features characterizing topological matter. Examples now include response of wave functions under changing boundary conditions (Chern number), properties with respect to protecting symmetry (MPS order parameters), and nonlocal entanglement content of wave functions (disconnected entropies).

B. Conclusions

We have shown how the entanglement of disconnected partitions uniquely distinguishes topological superconducting phases in 1D systems. This distinction is naturally interpreted within a lattice gauge theory framework and leads to key footprints both at the ground state level and in quantum quenches. Entanglement order parameters display universal scaling behavior when crossing phase transitions, characterized by entanglement critical exponents. Our findings show that modest partition sizes—of the order of what has been already experimentally demonstrated—are sufficient to uniquely characterize topological superconductors via entanglement. It would be intriguing to investigate whether other forms of quantum correlations between disconnected partitions, such as discord

[54] or quantum coherences [55], display similar characteristic features and if entanglement topological invariants can be used to characterize the real-time dynamics of interesting topological matter [43].

ACKNOWLEDGMENTS

We thank S. Barbarino, G. Giudici, F. Illuminati, N. Lindner, L. Pastori, D. Schuricht, F. Surace, X. Turkeshi, and B. Vermersch for useful discussions, and J. Budich for suggesting the investigation of the real-time dynamics. This work is partly supported by the ERC under Grant No. 758329 (AGEnTh) and has received funding from the European Union's Horizon 2020 research and innovation program under Grant Agreement No 817482. G.M. is partially supported through the project QUANTUM by Istituto Nazionale di Fisica Nucleare (INFN) and through the project ALMAIDEA by University of Bologna.

APPENDIX A: ADDITIONAL INFORMATION ON THE KITAEV MODEL

In this Appendix, we briefly present the Kitaev model and detail the derivation of all the analytical results mentioned in the main text. More specifically, we focus on the regime described in Kitaev's original paper [24] whose algebra is simpler while containing important features on the entanglement properties of the whole model when it displays a topological phase.

1. The Kitaev model without interaction

We give here a brief reminder of the Kitaev wire of Kitaev's seminal paper [24] for the unfamiliar reader. The Kitaev wire is a chain of L spinless fermions with OBCs described by the Hamiltonian

$$H = \sum_{j=1}^{L-1} \left(-t(a_j^\dagger a_{j+1} + a_{j+1}^\dagger a_j) - \mu \left(a_j^\dagger a_j - \frac{1}{2} \right) + \Delta a_j a_{j+1} + \Delta^* a_{j+1}^\dagger a_j^\dagger \right), \quad (\text{A1})$$

where t is the hopping amplitude, μ is the chemical potential, and $\Delta = |\Delta|e^{i\theta}$ the induced superconducting gap. It is convenient to absorb the complex phase of the latter in a (completely local) redefinition of the local creation and annihilations operators a_j^\dagger and a_j such that

$$(a_j^\dagger, a_j) \rightarrow (e^{-i\theta/2} a_j^\dagger, e^{i\theta/2} a_j), \quad (\text{A2})$$

and consider Eq. (A1) with Δ real only. It is then useful to introduce the Majorana fermions operators c_j (for $j = 1, \dots, L$),

$$c_{2j-1} = a_j + a_j^\dagger, \quad c_{2j} = \frac{a_j - a_j^\dagger}{i}, \quad (\text{A3})$$

such that

$$\{c_m, c_l\} = 2\delta_{m,l}, \quad c_m^\dagger = c_m, \quad (\text{A4})$$

where $\delta_{m,l}$ is the Kronecker delta. The Hamiltonian Eq. (A1) then becomes

$$H = \frac{i}{2} \sum_{j=1}^{L-1} (-\mu c_{2j-1} c_{2j} + (t + |\Delta|) c_{2j} c_{2j+1} + (-t + |\Delta|) c_{2j-1} c_{2j+2}). \quad (\text{A5})$$

In the special regime of parameters when $|\Delta| = t > 0$ and $\mu = 0$ (which we call the stereotypical regime), the Hamiltonian Eq. (A5) becomes

$$H = it \sum_{j=1}^{L-1} c_{2j} c_{2j+1}, \quad (\text{A6})$$

where it is important to note that the Majorana operators appearing in each term of the sum are not from the same sites. One can define local fermionic creation and annihilation operators on the link such that (for $j = 1, \dots, L-1$ only)

$$\tilde{a}_j = \frac{c_{2j} + ic_{2j+1}}{2}, \quad \tilde{a}_j^\dagger = \frac{c_{2j} - ic_{2j+1}}{2}, \quad (\text{A7})$$

that only mixes two neighboring sites. The Hamiltonian Eq. (A6) becomes diagonal,

$$H = 2t \sum_{j=1}^{L-1} \left(\tilde{a}_j^\dagger \tilde{a}_j - \frac{1}{2} \right), \quad (\text{A8})$$

and has two degenerate ground states, each pairing a Majorana fermion of one edge with a Majorana fermion of the other (cf. Fig. 8). Defining the nonlocal operators,

$$b = \frac{c_{2L} + ic_1}{2}, \quad b^\dagger = \frac{c_{2L} - ic_1}{2}, \quad (\text{A9})$$

the two ground states $|0\rangle$ and $|1\rangle$ satisfy

$$\forall j \in \llbracket 1, L-1 \rrbracket, \quad \tilde{a}_j |0\rangle = 0, \quad (\text{A10a})$$

$$\forall j \in \llbracket 1, L-1 \rrbracket, \quad \tilde{a}_j |1\rangle = 0, \quad (\text{A10b})$$

$$b |0\rangle = 0, \quad (\text{A10c})$$

$$b^\dagger |0\rangle = |1\rangle. \quad (\text{A10d})$$

In the case of periodic boundary conditions, $|0\rangle$ becomes the only ground state.



FIG. 8. The Kitaev chain with L sites and open boundary conditions. Each site i (denoted by a dashed circle) can be occupied by one spinless fermion and can be decomposed into two Majorana fermions (denoted by black dots) in $2i-1$ and $2i$. Associating the Majoranas $2i$ and $2i+1$ allows the construction of a quasilocal fermionic basis denoted with tildes. The ground states in the topological stereotypical regime will see its neighboring Majorana fermions pairing up, so, in the tilted basis, each site is unoccupied. Only the two Majorana on the edges do not need to pair up.

2. The entanglement properties of the topological phase in the stereotypical regime

To understand the entanglement properties of this topological phase and analytically compute the disconnected entanglement entropy S^D , it is useful to compute any reduced density matrices for the ground states $|0\rangle$ and $|1\rangle$ obtained in the stereotypical regime when $|\Delta| = t > 0$ and $\mu = 0$. To do so, it is useful to rewrite these states in the ‘‘second quantization’’ formalism, but in the tilted basis, where

$$\forall j \in \llbracket 1, L-1 \rrbracket, \quad \tilde{n}_j = \tilde{a}_j^\dagger \tilde{a}_j, \quad (\text{A11a})$$

$$n_b = b^\dagger b, \quad (\text{A11b})$$

where the index b stands for boundary. In that case, the two ground states can be rewritten as

$$|0\rangle = |\tilde{n}_1 = 0, \tilde{n}_2 = 0, \dots, \tilde{n}_{j-1} = 0, n_b = 0\rangle, \quad (\text{A12a})$$

$$|1\rangle = |\tilde{n}_1 = 0, \tilde{n}_2 = 0, \dots, \tilde{n}_{j-1} = 0, n_b = 1\rangle, \quad (\text{A12b})$$

which is a quasilocal basis in the sense that each \tilde{n}_j can be expressed in terms of operators acting only on sites j and $j+1$. For a connected bipartition of the system, as illustrated in Fig. 9, the ground states [Eqs. (A12)] cannot be written as a product state, due to both the presence of edge states and the way Majorana fermions are linked in the bulk of the system (for instance, see link $c \in \llbracket 1, L-1 \rrbracket$ of Fig. 9).

To properly do the partial trace and obtain the reduced density matrix ρ_A , it is better to express the ground states in terms of a local basis for both A and B . This becomes possible when rewriting the two parts of the open Kitaev wire as two open Kitaev wires connected into a singlet on the link c . Calling L_A the size of A , and L_B the size of B , such that $L_A + L_B = L$, we define a fermionic basis, local in A and B ,

$$a_A = \frac{1}{2}(c_{2L_A} + ic_1), \quad (\text{A13a})$$

$$a_A^\dagger = \frac{1}{2}(c_{2L_A} - ic_1), \quad (\text{A13b})$$

$$a_B = \frac{1}{2}(c_{2L_A+2L_B} + ic_{2L_A+1}), \quad (\text{A13c})$$

$$a_B^\dagger = \frac{1}{2}(c_{2L_A+2L_B} - ic_{2L_A+1}), \quad (\text{A13d})$$

$$\tilde{a}_c = \frac{1}{2}(c_{2L_A} + ic_{2L_A+1}), \quad (\text{A13e})$$

$$\tilde{a}_c^\dagger = \frac{1}{2}(c_{2L_A} - ic_{2L_A+1}), \quad (\text{A13f})$$

$$b = \frac{1}{2}(c_{2L} + ic_1), \quad (\text{A13g})$$

$$b^\dagger = \frac{1}{2}(c_{2L} - ic_1), \quad (\text{A13h})$$

so a_A and a_B (and Hermitian conjugate) act as boundary operators for the subchains A and B , respectively. Hence, in second quantization, and after dropping the redundant mentions of

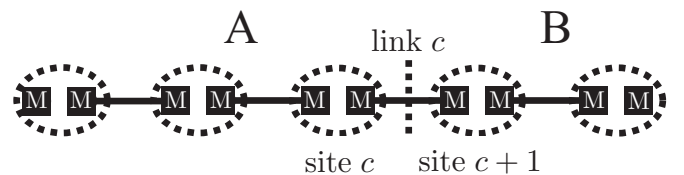


FIG. 9. A physical cut can only be done between sites, here, on the link c , partitioning the chain into two subsets: A and B .

the \tilde{n}_j , $j \in \llbracket 1, L-1 \rrbracket \setminus \{c = L_A\}$, the two ground states of the full chain are $|n_b = 0, \tilde{n}_c = 0\rangle$ and $|n_b = 1, \tilde{n}_c = 0\rangle$. The local basis of A and B is $\{|n_A, n_B\rangle\}$, where $n_A = a_A^\dagger a_A$ and $n_B = a_B^\dagger a_B$ take the values 0 or 1. Using Eqs. (A10) and (A13), we find

$$|n_b = 0, \tilde{n}_c = 0\rangle = -\frac{1}{\sqrt{2}}(|n_A = 1, n_B = 0\rangle - |n_A = 0, n_B = 1\rangle), \quad (= |0\rangle) \quad (\text{A14a})$$

$$|n_b = 1, \tilde{n}_c = 1\rangle = \frac{1}{\sqrt{2}}(|n_A = 1, n_B = 0\rangle + |n_A = 0, n_B = 1\rangle), \quad (\text{A14b})$$

$$|n_b = 1, \tilde{n}_c = 0\rangle = \frac{1}{\sqrt{2}}(|n_A = 0, n_B = 0\rangle + |n_A = 1, n_B = 1\rangle), \quad (= |1\rangle) \quad (\text{A14c})$$

$$|n_b = 0, \tilde{n}_c = 1\rangle = \frac{1}{\sqrt{2}}(-|n_A = 0, n_B = 0\rangle + |n_A = 1, n_B = 1\rangle). \quad (\text{A14d})$$

Tracing over B is immediate, as the only vectors of the basis of B with possible nonzero contributions are $|n_B = 0\rangle$ and $|n_B = 1\rangle$. In particular,

$$\rho_A(|n_b = 0, \tilde{n}_c = 0\rangle\langle n_b = 0, \tilde{n}_c = 0|) = \frac{1}{2}(|n_A = 1\rangle\langle n_A = 1| + |n_A = 0\rangle\langle n_A = 0|), \quad (\text{A15})$$

of entanglement entropy $S_A = \log 2$. The same happens for the other ground state.

Notice that the partial trace for fermions can induce a change of sign compared to the bosonic case. For example,

$$\text{Tr}_B(|n_A = 1, n_B = 1\rangle\langle n_A = 0, n_B = 1|) = -|n_A = 1\rangle\langle n_A = 0|. \quad (\text{A16})$$

Using Eqs. (A14), it is possible to get the expressions of the ground states in the local basis of an arbitrary partition. Additionally, taking a partition where all sites are their own individual subsets leads to the expression of the ground states in the original basis, up to a phase. The general expression of the reduced density matrix for an arbitrary partition of the system is obtained recursively, by considering the partition A_1, A_2, \dots, A_n of connected subsets A_i that are next to each other like in Fig. 10. Calling $A = A_1$ and $B = B_1 = \cup_{i=2}^n A_i$ allows use of Eqs. (A14) to express the two ground states in the local basis of A and B instead of $A \cup B$. The recurrence follows. Naming c_i the link between subsets A_i and A_{i+1} and constructing the ‘‘local boundary operators’’ a_{A_i} and $a_{A_i}^\dagger$ for



FIG. 10. A partition of the chain into n consecutive connected subsets A_1, A_2, \dots, A_n .

the subset A_i and a_{B_j} and $a_{B_j}^\dagger$ for $B_j = \cup_{i=j+1}^n A_i$, similarly to Eqs. (A14), the recurrence can be written as ($\forall n \geq 2$)

$$u_n(A_1, \dots, A_n), \quad (\text{A17a})$$

$$\doteq |n_b = 0, \tilde{n}_{c_1} = 0, \dots, \tilde{n}_{c_{n-1}} = 0\rangle (= |0\rangle), \quad (\text{A17b})$$

$$= \frac{1}{\sqrt{2}}(|n_{A_1} = 0, n_{B_1} = 1, \tilde{n}_{c_2} = 0, \dots, \tilde{n}_{c_{n-1}} = 0\rangle - |n_{A_1} = 1, n_{B_1} = 0, \tilde{n}_{c_2} = 0, \dots, \tilde{n}_{c_{n-1}} = 0\rangle), \quad (\text{A17c})$$

$$= \frac{1}{\sqrt{2}}(|n_{A_1} = 0\rangle \otimes v_{n-1}(A_2, \dots, A_n) - |n_{A_1} = 1\rangle \otimes u_{n-1}(A_2, \dots, A_n)), \quad (\text{A17d})$$

$$v_n(A_1, \dots, A_n), \quad (\text{A17e})$$

$$\doteq |n_b = 1, \tilde{n}_{c_1} = 0, \dots, \tilde{n}_{c_{n-1}} = 0\rangle (= |1\rangle), \quad (\text{A17f})$$

$$= \frac{1}{\sqrt{2}}(|n_{A_1} = 0, n_{B_1} = 0, \tilde{n}_{c_2} = 0, \dots, \tilde{n}_{c_{n-1}} = 0\rangle + |n_{A_1} = 1, n_{B_1} = 1, \tilde{n}_{c_2} = 0, \dots, \tilde{n}_{c_{n-1}} = 0\rangle), \quad (\text{A17g})$$

$$= \frac{1}{\sqrt{2}}(|n_{A_1} = 0\rangle \otimes u_{n-1}(A_2, \dots, A_n) + |n_{A_1} = 1\rangle \otimes v_{n-1}(A_2, \dots, A_n)). \quad (\text{A17h})$$

Calling

$$U_n = u_n + i v_n, \quad (\text{A18a})$$

$$V_n = u_n - i v_n, \quad (\text{A18b})$$

$$|+_j\rangle = 1/\sqrt{2}(i|n_{A_j} = 0\rangle - |n_{A_j} = 1\rangle), \quad (\text{A18c})$$

$$|-_j\rangle = 1/\sqrt{2}(-i|n_{A_j} = 0\rangle - |n_{A_j} = 1\rangle), \quad (\text{A18d})$$

these relations become

$$U_n(A_1, \dots, A_n) = |+_1\rangle \otimes V_{n-1}(A_2, \dots, A_n), \quad (\text{A19a})$$

$$= \begin{cases} |+_1 -_2 \dots -_{n-2}\rangle \otimes U_2(A_{n-1}, A_n) & \text{if } n \text{ is even} \\ |+_1 -_2 \dots +_{n-2}\rangle \otimes V_2(A_{n-1}, A_n) & \text{if } n \text{ is odd,} \end{cases} \quad (\text{A19b})$$

$$V_n(A_1, \dots, A_n) = |-_1\rangle \otimes U_{n-1}(A_2, \dots, A_n), \quad (\text{A19c})$$

$$= \begin{cases} |-_1 +_2 \dots +_{n-2}\rangle \otimes V_2(A_{n-1}, A_n) & \text{if } n \text{ is even} \\ |-_1 +_2 \dots -_{n-2}\rangle \otimes U_2(A_{n-1}, A_n) & \text{if } n \text{ is odd,} \end{cases} \quad (\text{A19d})$$

where

$$u_2(A_{n-1}, A_n) = \frac{1}{\sqrt{2}}(|n_{A_{n-1}} = 0, n_{A_n} = 1\rangle - |n_{A_{n-1}} = 1, n_{A_n} = 0\rangle), \quad (\text{A20a})$$

$$v_2(A_{n-1}, A_n) = \frac{1}{\sqrt{2}}(|n_{A_{n-1}} = 0, n_{A_n} = 0\rangle + |n_{A_{n-1}} = 1, n_{A_n} = 1\rangle), \quad (\text{A20b})$$

so

$$U_2(A_{n-1}, A_n) = \sqrt{2}i|+_1 -_1\rangle, \quad (\text{A21a})$$

$$V_2(A_{n-1}, A_n) = \sqrt{2}i|+_1 +_1\rangle. \quad (\text{A21b})$$

Therefore, in a local basis of A_1, \dots, A_n , the ground states become

$$|n_b = 0\rangle = u_n(A_1, \dots, A_n) \quad (\text{A22a})$$

$$= \frac{i}{\sqrt{2}}(|+1 -2 \dots\rangle + |-1 +2 \dots\rangle), \quad (\text{A22b})$$

$$|n_b = 1\rangle = v_n(A_1, \dots, A_n) \quad (\text{A22c})$$

$$= \frac{i}{\sqrt{2}}(|+1 -2 \dots\rangle - |-1 +2 \dots\rangle). \quad (\text{A22d})$$

These states are not Néel states because they are made out of fermions. It becomes clear in the basis of the subsets $\{\otimes |n_{A_j}\rangle\}_j$ up to the global phase change:

$$|\tilde{0}_j\rangle \doteq (-1)^j i |0_{A_j}\rangle \quad \text{and} \quad |\tilde{1}_j\rangle \doteq |1_{A_j}\rangle. \quad (\text{A23})$$

In that case,

$$|+1 -2 \dots\rangle = \left(-\frac{1}{\sqrt{2}}\right)^n \otimes_{i=1}^n [|\tilde{0}_i\rangle + |\tilde{1}_i\rangle], \quad (\text{A24a})$$

$$= \left(-\frac{1}{\sqrt{2}}\right)^n \sum_{\{n_{A_i}\}_{i \in [1, n]} = 0, 1} |\{n_{A_i}\}_{i \in [1, n]}\rangle, \quad (\text{A24b})$$

$$|-1 +2 \dots\rangle = \left(-\frac{1}{\sqrt{2}}\right)^n \times \sum_{\{n_{A_i}\}_{i \in [1, n]} = 0, 1} (-1)^{n - \sum n_{A_i}} |\{n_{A_i}\}_{i \in [1, n]}\rangle, \quad (\text{A24c})$$

so

$$S_{A_1 \cup A_3 \cup A_5 \cup \dots} = \left\lfloor \frac{n+1}{2} \right\rfloor \log 2, \quad (\text{A25})$$

where $\lfloor \dots \rfloor$ is the floor function, and n the number of partition. This last equation proves the exact additivity of the entropy in this case independently of the position of the cuts, which, in addition to the non-nullity of the contribution of the individual subsets, ensure the non-nullity of S^D for any superposition of the ground states. Indeed, for $n = 4$,

$$S^D = S_{A_1 \cup A_2} + S_{A_2 \cup A_4} - S_{A_2} - S_{A_1 \cup A_2 \cup A_4}, \quad (\text{A26})$$

becomes the net contribution of one connected subset only: $\log 2$. Alternatively, it is the contribution of two cut Bell pairs of Majorana fermions. This result is valid for both the von Neumann and the Rényi entropies.

3. Equivalence of the S_n^D

For 1D gapped systems, all S_n^D can be used interchangeably, with $n \geq 1$ and finite the index of the Rényi entropy:

(i) The property of minimum value shared by all S_n imply that if $S_{n_1} \neq 0$, then $S_{n_2} \neq 0$ and vice versa, so both are simultaneously nonzero.

(ii) The property of monotonicity and the fact that all gapped 1D phases have finite von Neumann entanglement entropy imposes all S_n to also be finite for 1D gapped systems, so no S_n^D can diverge.

(iii) For a given n entropy, translation invariance further imposes that all connected entropy will have the same value for big subset size, i.e., if A_{i+t} is the subset translated from A_i , then $S_n(A_{i+t}) = S_n(A_i)$ up to finite size effects.

(iv) The property of additivity is shared by all S_n .

4. Comparison between the topological and nontopological phases away from the phase transition

In the topological superconductor phase, away from any phase transition, both the von Neuman and Rényi entanglement entropies for large enough partitions (i.e., $L_A, L_B, L_D \gg \xi$ for the definitions of Fig. 1(a), or $L_{A_i} \gg \xi$ for all i for Eq. (A26) are nonzero and additive as demonstrated above in the stereotypical regime (in addition, see next section). If A is a simply connected subset of a partition of the chain (independent of its position), then, $S_A = 2\Gamma$, where $\Gamma = (\log 2)/2$ is the contribution of one (Majorana) Bell pair. Eq. (A26) then gives

$$S^D = 2\Gamma + 2 \times 2\Gamma - 2\Gamma - 2\Gamma = 2\Gamma. \quad (\text{A27})$$

In that regard, S^D is not unique: Combinations such as $S_{A_1 \cup A_3} + S_{A_2 \cup A_4} - S_{A_1 \cup A_4} - S_{A_2 \cup A_3}$ would have also work as detectors, but with less experimental relevance and a more complicated interpretation in terms of mutual information. The quantitative equality $S^D = S_n^D$ is here coincidental and is not a generic feature for other systems.

For the band insulator phase and for large enough partitions, the contribution of each term of Eq. (A26) is proportional to the number of boundaries of the partition, as we expect from the so-called *area law*. For the 1D OBC systems, one can argue that $S^D = 0$ by simply counting the number of boundaries of the partitions shown in Fig. 1(a), which gives

$$S^D = \Theta + 3\Theta - 2\Theta - 2\Theta = 0, \quad (\text{A28})$$

where Θ is the contribution for the entanglement of a single boundary. While Θ is model-parameter depending, the ratios between each terms are constant in the limit $L_A, L_B, L_D \gg \xi$, ensuring $S^D = 0$. In the limit $\mu \rightarrow \infty$, each term is identically zero. The result $S^D = 0$ in the nontopological phase is backed up by numerical simulations.

We also discuss the behavior of S^D for other nontopological phases. For the case of a gapped phase displaying ground state equivalent to, e.g., a maximally entangled Néel state, the entanglement entropy becomes nonzero for each term, but is not additive, such that (calling Θ the contribution of the only Bell pair of spin 1/2)

$$S^D = \Theta + \Theta - \Theta - \Theta = 0. \quad (\text{A29})$$

For a critical phase, conformal field theory predicts a vanishing contribution. This is in agreement with all of our microscopic simulations. For critical, nonconformal points, we are not aware of any field theoretical prediction.

Finally, for the case of a rigorously dimerized phase, S^D is well-defined and can be considered additive, but is not translation invariant. More precisely, let us define ϵ_{ij} , where $i, j = 1, 2, 3, 4$, such that $\epsilon_{ij} = 1$ if the cut between A_i and

A_j is on a dimer, and $\epsilon_{ij} = 0$ otherwise. Then, if Θ is the contribution of one dimer,

$$\begin{aligned} S^D &= \Theta(\epsilon_{41} + \epsilon_{23} + \epsilon_{12} + \epsilon_{23} + \epsilon_{34} + \epsilon_{41} \\ &\quad - \epsilon_{12} - \epsilon_{23} - \epsilon_{23} - \epsilon_{34}) \\ &= 2\Theta\epsilon_{41}, \end{aligned} \quad (\text{A30})$$

which is always zero if A_1 and A_4 are subsets at both ends of the open chain. S^D is not translation invariant in the case of periodic boundary conditions.

APPENDIX B: ADDITIONAL INFORMATION ON THE NUMERICAL METHODS

1. Computation using free-fermion correlation functions at equilibrium

The main challenge of the numerical analysis consists of calculating the four von Neumann entanglement entropies that are included in the definition of the disconnected TEE S^D of Eq. (1). We recall that each of these four quantities is associated with a specific possibly disconnected bipartition of the chain, following the scheme shown in Fig. 1(a).

The starting point for evaluating von Neumann or Rényi entanglement entropy S_A of a generic bipartition A and B (not necessarily simply connected) is the computation of the reduced density matrix $\rho_A = \text{Tr}_B|\psi\rangle\langle\psi|$, where $|\psi\rangle$ is a ground state of the whole system. For the Kitaev wire without interactions, i.e., when $U = 0$, the Hamiltonian Eq. (A1) is a free-fermion Hamiltonian that only conserves fermion number parity. It can be diagonalized by a Bogoliubov transformation. The reduced density matrix ρ_A of a generic partition can be interpreted as the thermal density matrix at temperature $T = 1$ for an entanglement Hamiltonian \mathcal{H}_A . Then $\rho_A = Z_A^{-1}e^{-\mathcal{H}_A}$ with $Z_A = \text{Tr}[e^{-\mathcal{H}_A}]$ [56–58]. It is then possible to compute ρ_A of a generic partition by following the well-established approach of Ref. [38]. The first step of this very general procedure is the computation of the correlation matrices in the original ground state: $C_{nm} = \langle\psi|a_n^\dagger a_m|\psi\rangle$ and $F_{nm} = \langle\psi|a_n^\dagger a_m^\dagger|\psi\rangle$, where n and m run over the sites of the subset A . At equilibrium, F_{nm} is real, so the spectrum of the entanglement Hamiltonian can be determined by numerically solving the eigenvalue problem [38]:

$$(2\hat{C} - 2\hat{F} - 1)(2\hat{C} + 2\hat{F} - 1)\phi_l = \tanh^2\left(\frac{\epsilon_l}{2}\right)\phi_l. \quad (\text{B1})$$

ϵ_l are the eigenvalues of the entanglement Hamiltonian with eigenvectors ϕ_l . Once the spectrum ϵ_l is obtained, we can easily compute the reduced density matrix ρ_A and the entanglement entropy of any bipartition, connected or not.

We carried out these numerical calculations with arbitrary precision by using MPMATH Python library [59]. Two requirements arise: Avoiding numerical precision problems when the eigenvalues of the left side of Eq. (B1) are approximately 0 and avoiding divergence problems when they are very close to 1. These issues are fixed by taking a number of digits proportional to the total size of the system L : We set $\text{mp.dps} = 20 \times L$ (number of digits in the Python library). While the approach allows generation of a lot of data with relatively little cost, the interaction case, as well as the bilinear

biquadratic model remain inaccessible with this algorithm. Instead, we have to switch to the DMRG technique presented Appendix B 3.

2. Sudden quenches using free-fermion correlation functions

We check that S^D is a topological invariant by looking at its time evolution after sudden quenches. The system starts in its ground state before the quench, for a given set of parameters of the Hamiltonian. At $t = 0$, we change the value of one of these parameters. We then let the system evolve in time.

The generic interacting case is very challenging to follow because the interacting term induces a time evolution of an extensive number of eigenstates of the spectrum. For the free-fermion case, the same previous numerical approach of Appendix B 1 still applies with the same efficiency. The matrix F_{nm} is, however, complex during the time evolution of the system so Eq. (B1) is not valid anymore. We follow instead Ref. [60] and use the definition of the Majorana fermions of Eq. (A2). The relevant $2L \times 2L$ correlation matrix is this time $M_{nm} = \langle c_n c_m \rangle$, rewritten as $M_{nm} = \delta_{nm} + \Gamma_{nm}$ with n, m the (half-)site indices spanning only the relevant subset studied. The eigenvalues of Γ_{nm} are $\pm \tanh \epsilon_l/2$, with ϵ_l the entanglement energies of the reduced density matrix associated with the subset. The time dependent matrix Γ_{nm} is directly linked to the time-dependent Hamiltonian analytically, and then diagonalized numerically, similar to Ref. [61].

We performed several quenches of different amplitudes inside both the TSC and the band insulator, as well as across the phase transition, as seen in Fig. 6. S^D is plotted as a function of time for different chain lengths L with $L/L_A = 4$, $L_A = L_B$, using the same definition of Fig. 1(a) for the partitions. Figs. 6(a)–6(c) exhibit a quantized finite plateau depending on L_A . We define the time size of the plateau with t_c : The time at which S^D deviates from $\log 2$ to $0.95 \log 2$. t'_c is time of revival, when S^D increases from 0 to $0.05 \log 2$. We plot $1/t_c$ or $4/t'_c$ in Figs. 6(d)–6(f) as a function of $1/L$. The linear extrapolations of the length of the plateau show divergences of both time sizes when $L \rightarrow \infty$ for each kind of quench: S^D stays quantized in the thermodynamical limit because the drops/revivals are only finite-size effects. Thus, S^D does not change under coherent time evolution and behaves as a topological invariant.

We used the same implementation as in Appendix B 1 with $\text{mp.dps} = 3 \times L$, enough to get reliable results.

3. Computation using DMRG

For the case of the interacting Kitaev wire with $U \neq 0$ [Eq. (2)], the numerical study is now carried out with the DMRG algorithm formulated in the MPS language [62].

The main challenge is again the computation of von Neumann or Rényi entanglement entropies of disconnected bipartitions of the chain to determine the behavior of S^D of Eq. (1). For DMRG, however, only the standard connected bipartition of the MPS state into two halves is very efficient. This efficiency comes from the intimate structure of an MPS

state and the use of left-/right-orthogonality condition [62]. The MPS tensors themselves already give the eigenstates of the reduced density matrix of a block of sites starting from either the left or the right edge of the system. Instead, for generic bipartitions of the chain, such as partitions B , $A \cup B$, or $A \cap B$ of Fig. 1(a), the calculation of the reduced density matrix is highly nontrivial as it involves several multi-index tensor contractions. As a result, the computational cost scales exponentially with the size of the subset.

We circumvent this numerical problem by reordering the MPS sites appropriately, thus considering a long-range Hamiltonian reproducing the original model. Two rearrangements are necessary, as shown in Fig. 11. (i) is a circular permutation of the original multipartitions to efficiently calculate $S(\rho_A)$, $S(\rho_{A \cup B})$, and $S(\rho_{A \cap B})$ because all these quantities are now related to the rightmost bipartitions of the chain. In the process, we only reindex the sites while their respective connectivity is left unchanged. (ii) allows computation of $S(\rho_B)$. In this way, we efficiently obtain the four entanglement entropies composing S^D .

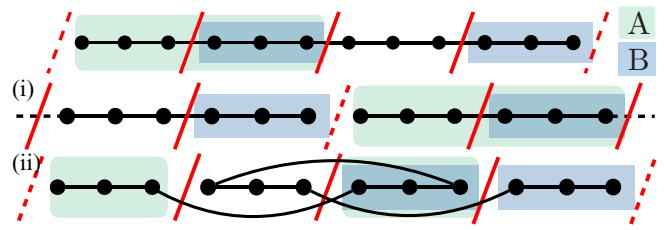


FIG. 11. Scheme of the partitions. Two “tricks” are used to compute only standard bipartition of the chain: (i) a circular permutation of the partition used for $S(\rho_A)$, $S(\rho_{A \cup B})$, and $S(\rho_{A \cap B})$ and (ii) reindexing the sites, thus making the Hamiltonian long range, but making the subset B connected and used for $S(\rho_B)$.

In our numerical analysis with DMRG algorithm, we used a bond dimension up to 1200, a truncation error of 10^{-8} , and at least 30 sweeps to reach the convergence and to ensure stability of our findings. We noticed that along the Peschel-Emery line of Ref. [23] in the TSC phase, S^D converge even faster to its quantized value of $\log 2$.

- [1] L. Amico, R. Fazio, A. Osterloh, and V. Vedral, *Rev. Mod. Phys.* **80**, 517 (2008).
- [2] P. Calabrese and J. Cardy, *J. Phys. A: Math. Theor.* **42**, 504005 (2009).
- [3] J. Eisert, M. Cramer, and M. B. Plenio, *Rev. Mod. Phys.* **82**, 277 (2010).
- [4] E. Fradkin, *Field Theories of Condensed Matter Systems* (Cambridge University Press, Cambridge, 2013).
- [5] A. Hamma, R. Ionicioiu, and P. Zanardi, *Phys. Lett. A* **337**, 22 (2005).
- [6] M. Levin and X.-G. Wen, *Phys. Rev. Lett.* **96**, 110405 (2006).
- [7] A. Kitaev and J. Preskill, *Phys. Rev. Lett.* **96**, 110404 (2006).
- [8] X.-G. Wen, *Science* **363**, eaal3099 (2019).
- [9] S. Depenbrock, I. P. McCulloch, and U. Schollwöck, *Phys. Rev. Lett.* **109**, 067201 (2012).
- [10] H.-C. Jiang, Z. Wang, and L. Balents, *Nat. Phys.* **8**, 902 (2012).
- [11] S. V. Isakov, M. B. Hastings, and R. G. Melko, *Nat. Phys.* **7**, 772 (2011).
- [12] D. A. Abanin and E. Demler, *Phys. Rev. Lett.* **109**, 020504 (2012).
- [13] A. J. Daley, H. Pichler, J. Schachenmayer, and P. Zoller, *Phys. Rev. Lett.* **109**, 020505 (2012).
- [14] A. Elben, B. Vermersch, M. Dalmonte, J. I. Cirac, and P. Zoller, *Phys. Rev. Lett.* **120**, 050406 (2018).
- [15] B. Vermersch, A. Elben, M. Dalmonte, J. I. Cirac, and P. Zoller, *Phys. Rev. A* **97**, 023604 (2018).
- [16] H. Pichler, G. Zhu, A. Seif, P. Zoller, and M. Hafezi, *Phys. Rev. X* **6**, 041033 (2016).
- [17] M. Dalmonte, B. Vermersch, and P. Zoller, *Nat. Phys.* **14**, 827 (2018).
- [18] E. Cornfeld, E. Sela, and M. Goldstein, *Phys. Rev. A* **99**, 062309 (2019).
- [19] F. Pollmann, A. M. Turner, E. Berg, and M. Oshikawa, *Phys. Rev. B* **81**, 064439 (2010).
- [20] L. Fidkowski, *Phys. Rev. Lett.* **104**, 130502 (2010).
- [21] A. M. Turner, F. Pollmann, and E. Berg, *Phys. Rev. B* **83**, 075102 (2011).
- [22] Examples include the equivalence between the entanglement spectra of the ground state of finite Ising and Kitaev chains, and spin ladders [19].
- [23] H. Katsura, D. Schuricht, and M. Takahashi, *Phys. Rev. B* **92**, 115137 (2015).
- [24] A. Y. Kitaev, *Phys.-Usp.* **44**, 131 (2001).
- [25] C. Beenakker, *Ann. Rev. Cond. Matt. Phys.* **4**, 113 (2013).
- [26] T. Brydges, A. Elben, P. Jurcevic, B. Vermersch, C. Maier, B. P. Lanyon, P. Zoller, R. Blatt, and C. F. Roos, *Science* **364**, 260 (2019).
- [27] S. J. van Enk and C. W. J. Beenakker, *Phys. Rev. Lett.* **108**, 110503 (2012).
- [28] H. Casini and M. Huerta, *Phys. Lett. B* **600**, 142 (2004).
- [29] D. Wang, S. Xu, Y. Wang, and C. Wu, *Phys. Rev. B* **91**, 115118 (2015).
- [30] B. Zeng and D. L. Zhou, *EPL* **113**, 56001 (2016).
- [31] I. H. Kim, *Phys. Rev. B* **89**, 235120 (2014).
- [32] E. M. Stoudenmire, J. Alicea, O. A. Starykh, and M. P. Fisher, *Phys. Rev. B* **84**, 014503 (2011).
- [33] M. Caraglio and F. Gliozzi, *J. High Energy Phys.* **11** (2008) 076.
- [34] S. Furukawa, V. Pasquier, and J. Shiraishi, *Phys. Rev. Lett.* **102**, 170602 (2009).
- [35] B. M. McCoy and M.-L. Yan, *Nuc. Phys. B* **215**, 278 (1983).
- [36] C. Lacroix, P. Mendels, and F. Mila (eds.), *Introduction to Frustrated Magnetism*, Springer Series in Solid-State Sciences Vol. 164, (Springer-Verlag, Berlin, Heidelberg, 2010).
- [37] B. Zeng, X. Chen, D.-L. Zhou, and X.-G. Wen, *Quantum Information Meets Quantum Matter* (Springer, New York, 2019).
- [38] I. Peschel, *J. Phys. A: Math. Gen.* **36**, L205 (2003).
- [39] S. R. White, *Phys. Rev. Lett.* **69**, 2863 (1992).
- [40] U. Schollwöck, *Rev. Mod. Phys.* **77**, 259 (2005).
- [41] M. D. Caio, N. R. Cooper, and M. J. Bhaseen, *Phys. Rev. Lett.* **115**, 236403 (2015).
- [42] L. D’Alessio and M. Rigol, *Nat. Commun.* **6**, 8336 (2015).

- [43] M. McGinley and N. R. Cooper, *Phys. Rev. Res.* **1**, 033204 (2019).
- [44] T. Giamarchi, *Quantum Physics in One Dimension*, International Series of Monographs on Physics (Clarendon Press, Oxford, 2004).
- [45] N. M. Gergs, L. Fritz, and D. Schuricht, *Phys. Rev. B* **93**, 075129 (2016).
- [46] L. Levy and M. Goldstein, *Universe* **5**, 33 (2019).
- [47] Q. Niu, D. J. Thouless, and Y.-S. Wu, *Phys. Rev. B* **31**, 3372 (1985).
- [48] X. Chen, Z.-C. Gu, Z.-X. Liu, and X.-G. Wen, *Science* **338**, 1604 (2012).
- [49] J. Haegeman, D. Perez-Garcia, I. Cirac, and N. Schuch, *Phys. Rev. Lett.* **109**, 050402 (2012).
- [50] F. Pollmann and A. M. Turner, *Phys. Rev. B* **86**, 125441 (2012).
- [51] H. Shapourian, K. Shiozaki, and S. Ryu, *Phys. Rev. Lett.* **118**, 216402 (2017).
- [52] H. Shapourian, K. Shiozaki, and S. Ryu, *Phys. Rev. B* **95**, 165101 (2017).
- [53] A. Elben, J. Yu, G. Zhu, M. Hafezi, F. Pollmann, P. Zoller, and B. Vermersch, [arXiv:1906.05011](https://arxiv.org/abs/1906.05011) (2019).
- [54] H. Ollivier and W. H. Zurek, *Phys. Rev. Lett.* **88**, 017901 (2001).
- [55] I. Frérot and T. Roscilde, *Phys. Rev. B* **94**, 075121 (2016).
- [56] I. Peschel and M.-C. Chung, *J Phys. A: Math. Gen.* **32**, 8419 (1999).
- [57] M.-C. Chung and I. Peschel, *Phys. Rev. B* **62**, 4191 (2000).
- [58] M.-C. Chung and I. Peschel, *Phys. Rev. B* **64**, 064412 (2001).
- [59] F. Johansson and others, mpmath: A Python library for arbitrary-precision floating-point arithmetic, version 0.18, <http://mpmath.org/>.
- [60] I. Peschel and V. Eisler, *J. Phys. A: Math. Theo.* **42**, 504003 (2009).
- [61] M. Fagotti and P. Calabrese, *Phys. Rev. A* **78**, 010306(R) (2008).
- [62] U. Schollwöck, *Ann. Phys.* **326**, 96 (2011).